Convection-UNet: A Deep Convolutional Neural Network for Convection Detection based on the Geo High-speed Imager of Fengyun-4B

1st Yufei Wang
The State Key Laboratory of Management and Control for Complex Systems, Institute of Automation, Chinese Academy of Sciences & University of Chinese Academy of Sciences
Beijing, China
wangyufei2020@ia.ac.cn

2nd Baihua Xiao*
The State Key Laboratory of Management and Control for Complex Systems, Institute of Automation, Chinese Academy of Sciences
Beijing, China
baihua.xiao@ia.ac.cn

***Abstract*—Deep convection can cause a variety of severe weather conditions such as thunderstorms, strong winds, and heavy rainfall. Satellite observations provide all-weather and multi-directional observations, facilitating the timely detection of such weather systems, which is crucial to saving lives and property. However, previous methods based on channel feature extraction and threshold filtering did not make full use of information in satellite images, which led to limitations on such complex problems as strong convection detection. In this study, we propose a novel framework of a deep learning-based model Convection-UNet to detect convection. We use channel 4 to 7 of FY-4B GHI that we select according to the microphysical properties of convection as input and radar reflectivity as label. We combine the detailed training time and test time data augmentation strategies and build a deep neural network to automatically extract spatial context features and achieve end-to-end learning. Results show that the performance of our method far exceeds the previous channel extraction combined with threshold filtering methods such as BT and BTD at least 0.24 on F_1-measure. We also show that our channel selection and data augmentation strategies are of great significance to detect convection.**

Keywords-component; Fengyun-4B geostationary satellite, radar reflectivity, deep learning, data augmentation, cloud microphysical properties.

I. INTRODUCTION

The disaster weather caused by strong convection is always characterized by strong destruction, wide distribution, and rapid development, and is usually accompanied by severe weather events such as tornadoes heavy rainfall and flash flood, which poses a serious threat to human life and property safety[1–3]. Therefore, the detection of severe convective weather has attracted extensive attention. Meteorological satellite observation is a top-down observation method. Meteorological satellites can generate images with high spatial and temporal resolution through receiving and measuring the radiation of the earth and its atmosphere and achieve all-weather and multi-directional meteorological observations. Thus, satellite observations become a powerful tool for detecting convection in areas with weak meteorological support such as complex terrain, no man's land and the upper atmosphere[4,5].

Over the past few decades, the detection of severe convection based on satellite imagery was mainly based on the spectral channel threshold method, that is, based on the microphysical properties of severe convection, the corresponding features are extracted from the spectral channel, and the threshold is set to achieve the detection of convection. Maddox[6] used the brightness temperature of the infrared channel (10.7μm) to detect the strong convective regions. Since the cloud top in the strong convective regions is high and the temperature is low, convective clouds appear bright white in the infrared imagery and are in strong contrast with the non-convective region. This method can be used day and night. However, the detection method with a single channel has limitations. Subsequent studies showed multi-channel methods are better. BTD (Brightness Temperature Difference)[7] used the brightness temperature difference between water vapor and infrared imagery to explore cloud top features and detect convection. SATCAST (Satellite Convection Analysis and Tracking)[8] proposed the "interest fields" for assessing growing cumulus by integrating the channel features and time trends of convection. UWCI (University of Wisconsin Convective Initiation)[9] proposed to use box averaging to calculate the average cooling rate of cloud tops in infrared channels, and established a convection forecasting system based on the cooling rate of cloud tops and cloud types, thus effectively integrating spatial information. The threshold selection method is usually based on different terrain, season, and historical data of previous severe convective weather[10].

The methods mentioned above can effectively incorporate the microphysical properties of convection and have good practical significance. However, the satellite data we used in this paper is the Geo High-speed Imager (GHI) of Fengyun 4B, which contains only 7 channels (shown in Table 1), lacks water vapor channels and part of infrared channels, resulting in less spectral information that can be used to identify convection. On the other hand, considering the complex and changeable characteristics of convective clouds, the traditional multi-channel threshold detection methods are limited by the feature extraction method and threshold selection strategy, which lead to the bottleneck of detection effect.

In recent years, deep learning has shined in computer vision tasks due to its powerful feature-extracting ability, which had attracted extensive attention from academic research[11]. Some meteorologists tried to use a deep neural network to detect and forecast convection. Lee et al.[12] proposed an Encoder-Decoder two-stage detection model based on visible and infrared channels. The visible channel was used to reflect the optical thickness of the cloud, while the infrared channel reflected the temperature of the cloud top. Under the condition of ensuring the recall rate, the detection results were greatly improved and had better interpretability. Kim et al.[13] used Convolutional Neural

Table 1. The specification of FY-4B GHI.

Channel	Wavelength (μm)	Spatial resolution (km)	Main application
1	0.45-0.75	0.25	Land surface, vegetation
2	0.445-0.495	0.5	Small molecule aerosol, true color synthesis
3	0.52-0.57	0.5	Aerosol, true color synthesis
4	0.62-0.67	0.5	Aerosol, true color synthesis
5	1.371-1.386	0.5	Cirrus
6	1.58-1.64	0.5	Low cloud/snow identification, water cloud/ice cloud identification
7	10.3-12.5	2	Clouds or surface temperature

Network (CNN) to detect overshooting tops. They first selected satellite images of visible and infrared channels of fixed size as input according to the usual size of overshooting tops, then used CNN to extract features and classify them. Compared with the threshold method and random forest method[14], it could significantly improve precision and recall. Lee et al.[15] extended Kim et al. 's method by adding more infrared channels as input, and tried 2D-CNN and 3D-CNN to fuse visible channel and infrared channel data, respectively, and achieved better detection results.

Based on the above analysis, we propose a deep convolutional neural network architecture named Convection-UNet to detect convection from FY-4B GHI data. We first select four channels as the input according to the microphysical properties of convection, then use the UNet[16] architecture to construct our Convection-UNet for pixel-level convection detection. Our Convection-UNet also contains a strong data augmentation strategy and uses radar reflectivity as label. The experimental results show that (1) our deep learning method has a significant improvement compared with the previous spectral channel threshold methods, (2) the input channels selected for the microphysical mechanism and data augmentation also play an important role.

The remainder of this paper proceeds as follows. Section II introduces the satellite data and the radar data used for model input and label respectively. Section III describes our network architecture and training strategy. Section IV analyzes the experimental results in detail. Finally, we present the main conclusions of this study in Section V.

II. DATA

A. Satellite data: Fengyun-4B

Fengyun-4B (FY-4B in short) is the second satellite in China's Fengyun-4 geostationary meteorological satellite series, which was successfully launched on June 3, 2021. The Geo High-speed Imager (GHI) installed on the satellite achieved the first observation with a spatial resolution of 250m and a time interval of 1min, which improved the ability of warning and forecasting of small and medium scale severe weather disasters[17,18]. Table 1 shows the specification of FY-4B GHI.

However, there is overlap between channels (for example, channels 1 to 4 are all visible channels, and the difference between these channels is very small), and the excessive input leads to high time consumption of data processing. On the other hand, channel selection should be highly correlated with convection to make full use of the potential of automatic feature extraction of CNN. Therefore, it is a very important task to select appropriate channels as the input of CNN. Convective clouds are usually characterized by thick, high cloud tops, low surface temperature at the cloud tops, and small ice particles with strong updrafts[19–21]. For FY-4B GHI data, these methods[19–21] and NASA's quick guide on convection[1] lead us to construct the following combination of features to describe convection: 0.64μm reflectivity (to measure the optical thickness of the cloud), 1.38μm/1.6μm (to measure the phase of the cloud, the larger the value, the more likely the cloud is to behave as ice particles, otherwise it will appear as water clouds), 10.8μm brightness temperature (to measure the height of the cloud top). Considering that the deep neural network can automatically extract features, we use DN values of 0.64μm, 1.38μm, 1.6μm and 10.8μm (corresponding to channels 4 to 7 in GHI) as input to automatically learn the complex features of convection through the network. All image resolutions are 2km (corresponding to 1000 × 900 pixels per image).

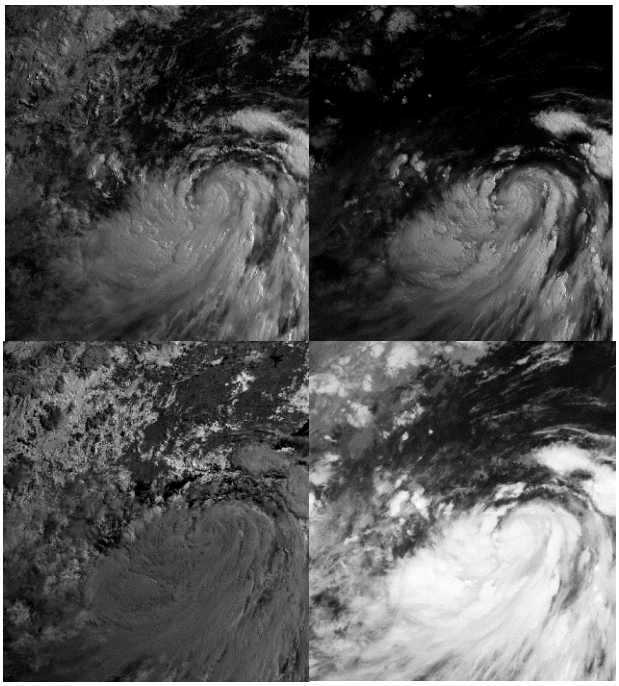

Figure 1. Image of FY-4B GHI at 0:00 UTC on July 1, 2022 (Channel 4 to 7 from top left to bottom right).

B. Radar data

The convection initiation determined by the threshold of radar reflectivity factor ≥ 35dBZ can be used to forecast the

[1]https://weather.msfc.nasa.gov/sport/training/quickGuides/rgb/QuickGuide_ConvectiveRGB_NASA_SPoRT.pdf

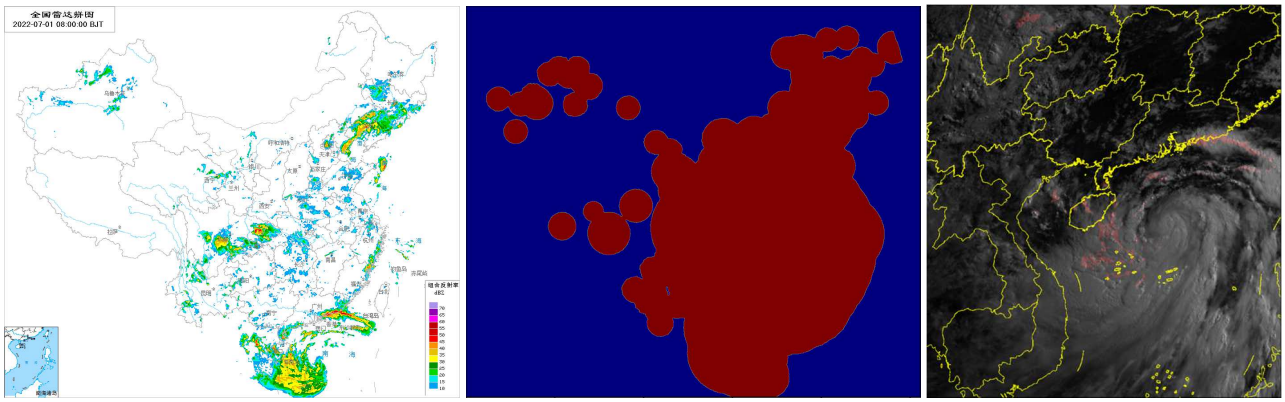

Figure 2. Schematic diagram of radar image analysis at 00:00 UTC time on July 1, 2022. The left figure shows the original 6-minute national radar mosaic. It should be noted some radar reflectivity values in Tibet, Xinjiang, and other regions in the left figure are blank not because the dBZ of these regions is less than 10, but because they are not covered by radar (the red areas in the middle figure indicate radar coverage areas, corresponding to the left figure). After the geographic information is analyzed from the radar mosaic and the projection transformation is carried out, the radar label at the corresponding time of the satellite data can be obtained (shown in the right figure, the red area is the radar reflectivity ≥ 35dBZ, while the yellow area is the auxiliary added national and provincial boundaries).

occurrences of severe weather events caused by convection in advance[22]. We use this standard as the identification criterion of convection and collect the national radar mosaic of China Central Meteorological Observatory at the corresponding time of satellite data. The frequency of the radar mosaic is 6 minutes, while the spatial resolution is about 4km. The radar coverage mainly covers most of the land and sea near the inland in China. We first process the radar mosaic, including clutter elimination, geographic information extraction, and projection transformation, to obtain the radar reflectivity results that match the satellite imagery in time and space, then generate pixel-level convection/non-convection binary supervision labels according to whether the reflectivity is ≥ 35dBZ.

C. Data processing

For the above four input satellite channels and matched radar supervision labels, we selected a total of 1508 images matched between July 1-7, 11-17, and 21-27, 2022 as the training set, and 111 images matched between June 11-17, 2022 as the test set. Before sending the data to the network, we processed the training satellite images as follows:

1. Mark abnormal areas: First, mark the pixels where the solar zenith angle is greater than 80°, then mark the pixels corresponding to the invalid area of radar (blue area of the second row in figure 2), The former operation avoids the influence of the abnormal value caused by the extreme solar zenith angle on the satellite imagery, while the latter process ensures that all satellite imagery pixels used for training have accurate labels based on radar reflectivity.
2. Numerical transformation: For the solar reflection channel (channel 4 to 6), the normalized reflectivity (the reflectivity divided by the cosine of the solar zenith angle) was calculated to replace the DN value. For the solar radiation channel (channel 7), the brightness temperature value is used instead of the DN value.
3. Normalization: the 1% and 99% quantiles of each channel in the training set were counted. Then the data is truncated and normalized to [0,1] to exclude possible outliers in satellite imagery.

Since there are always abnormal areas in the original 1000×900 pixel satellite images with 2km resolution, resulting in missing labels or abnormal data, it is necessary to cut them into small-size images. In this paper, we randomly crop 40 128×128 pixel images containing convection pixels but not any abnormal pixels from original images to better balance positive and negative samples and ensure the integrity of labels. We use the normalized values mentioned above as input to the model.

III. METHOD

A. Model

UNet[16] is a U-shaped end-to-end semantic segmentation network, which consists of a contracting path and an expansive path. The contracting path is equivalent to the Encoder to extract features and down-sampling images, while the expansive path is equivalent to the Decoder to automatically achieve pixel-level classification of original images through up-sampling and feature fusion which combines up-sampling results with the origin feature map from the contracting path at the same stage. We use bilinear interpolation for up-sampling to reduce the number of parameters and avoid overfitting. In the output phase, after the last convolution, the model is followed by a Sigmoid layer to predict the confidence score of convection.

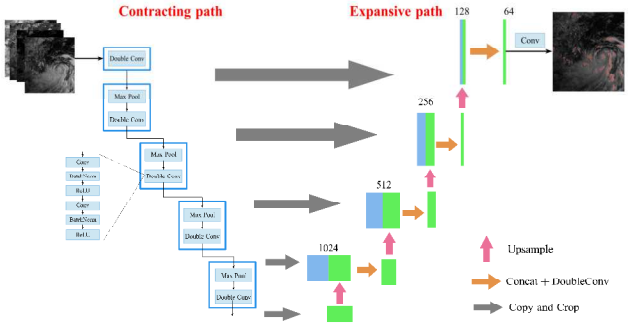

Figure 3. Convection-UNet network architecture.

B. Data augmentation

Data augmentation is an important part of model training. We follow nnUNet's[23] data augmentation strategy and divide data augmentation into training time augmentation and test time augmentation. Training time augmentation includes random flipping with a probability of 0.5, randomly adjusting image brightness and contrast

with a probability of 0.2, and randomly adding Gaussian noise and Gaussian blur with a probability of 0.2. Test time augmentation includes flip-weighted prediction and Gaussian smoothing prediction. Flip-weighted prediction can capture the spatial features of all directions comprehensively and obtain more robust prediction results by weighting the prediction results of various random flips of the image with equal weights. Gaussian smoothing prediction aims to better predict the category of pixels in the image boundary region. Considering that the original image is 1000×900 but the model input is 128×128, it is necessary to use a sliding window for prediction. However, the boundary pixels of the window usually lack spatial context information, resulting in poor prediction ability. Gaussian smoothing prediction uses partially overlapping sliding windows. We set the window size to 128×128, and the stride to 64, thus, each pixel will only be covered by one or two sliding windows. For the overlapping part in the sliding windows, the weighted prediction is adopted by $\hat{y}(x) = w_1 f(x, X_1) + w_2 f(x, X_2)$, where $\hat{y}(x)$ is the weighted prediction of pixel x, $f(x, X)$ represents the pixel x in the sliding window X, w is the weight of pixel x in sliding window X and obeys two-dimensional Gaussian distribution. The higher the weight near the middle, the lower the weight near the boundary.

C. Loss function

We use Dice Loss[24] (shown in Equation (1)) as loss function to train our model.

$$L = 1 - \frac{2 \times \mathrm{sum}(\boldsymbol{y} \cdot \hat{\boldsymbol{y}})}{\mathrm{sum}(\hat{\boldsymbol{y}}) + \mathrm{sum}(\boldsymbol{y})} \tag{1}$$

where $\boldsymbol{y}$ is the ground-truth of convection, $\hat{\boldsymbol{y}}$ is the confidence score of convection. Compared with binary cross-entropy loss, dice loss can better handle the imbalanced problem, which is more suitable for the task of convection detection (usually the number of convection pixels is far less than the number of non-convection pixels).

D. Experiment setting

The training and testing process of the model is as follows: in the training stage, we take the augmented results of 128×128 satellite images as input and send them to the network for training. We trained by Adam[25] with a minibatch size of 64 images, learning rate of 0.001, weight decay of 0.0001. Our model was trained and tested on 2 NVIDIA GTX 1080Ti GPUs. We trained for 200 epochs and saved the checkpoint for testing. In the test phase, we use the test time augmentation. After obtaining the confidence score through sigmoid function, we use 0.5 as the threshold to classify the convection.

IV. Results

We use precision, recall and F_1-measure as metrics to evaluate our model on test set, where precision is used to measure false positives, recall is used to measure missed detection and F_1-measure is the overall evaluation of precision and recall. These metrics are calculated by Equation (2-4).

$$\mathrm{Precision} = \frac{\mathrm{TP}}{\mathrm{TP} + \mathrm{FP}} \tag{2}$$

$$\mathrm{Recall} = \frac{\mathrm{TP}}{\mathrm{TP} + \mathrm{FN}} \tag{3}$$

$$\mathrm{F_1} = \frac{2 \times \mathrm{Precision} \times \mathrm{Recall}}{\mathrm{Precision} + \mathrm{Recall}} \tag{4}$$

where TP, FP and FN represent the number of hits, false alarms and misses.

We compared two spectral channel threshold methods, BT and BTD. BT[6] uses the brightness temperature of 10.8μm channel as the criterion for judging convection. We select three thresholds: 210K, 220K, and 230K, define the brightness temperature value less than the corresponding threshold as convection. BTD[7,26] uses the brightness temperature difference between water vapor (such as 6.25μm) and infrared imagery as the criterion for convection. Since FY-4B GHI does not have 6.25μm channel, we use the 6.25μm channel from FY-4B Advanced Geosynchronous Radiation Imager (AGRI) at the corresponding time for evaluation. We also select three thresholds: 0K, -5K, and -10K, and define pixels with channel difference greater than the corresponding threshold as convection.

Table 2. Comparison of different methods for convection detection.

Method	Precision	Recall	F_1-measure
BT < 210K	0.2273	0.2453	0.2360
BT < 220K	0.1483	0.4785	0.2264
BT < 230K	0.0955	0.6920	0.1679
BTD > 0K	0.4164	0.0171	0.0329
BTD > -5K	0.1547	0.5622	0.2426
BTD > -10K	0.0936	0.7634	0.1668
Convection-UNet (Ours)	0.4581	0.5293	**0.4911**

It can be seen from Table 2 that our Convection-UNet exceeds the detection methods based on channel threshold by a great advantage, and is at least 0.24 higher than the BT and BTD on F_1-measure. We believe that the performance of our method is improved mainly for two reasons: the increased number of channels and the design of end-to-end network architecture. The former provides more abundant data information, while the latter makes full use of the spatial context of satellite data. The integration of spatial information is intuitive in theory because the convection cloud usually presents a lumpy shape locally. The accuracy of previous methods based on the channel characteristics of a single pixel is limited since these methods ignore the information of the surrounding pixels. In addition, the network builds the feature extraction and threshold classification into an end-to-end architecture, which can automatically learn to construct the mapping of features and thresholds. However, in traditional methods such as BT and BTD, feature extraction and threshold classification are processed separately, which leads to a large semantic gap, so it is hard to deal with such a complex weather system as convection by using these methods.

We perform training time augmentation and test time augmentation for satellite images to improve the robustness of the model and avoid overfitting. The detailed results are shown in Table 3. When neither training time nor test time data augmentation is used, the F_1-measure on the test set is 0.4663. After adding training time augmentation or test time augmentation, F_1-measure is slightly increased to 0.4721

and 0.4768 respectively. Finally, when adding both training time augmentation and test time augmentation, F_1-measure rises to 0.4911. It can be seen that the effect of training time augmentation and test time augmentation is relatively obvious. Training time augmentation helps the model learn more data representation, enhance model robustness and avoid overfitting, while the flip-weighted prediction and Gaussian smoothing prediction in test time augmentation are similar to model ensemble, which can eliminate some uncertainties and abnormal predictions.

Table 3. Comparison of different data augmentation results.

Method	Precision	Recall	F_1-measure
No augmentation	0.4368	0.5001	0.4663
Add training time augmentation	0.4224	0.5350	0.4721
Add test time augmentation	0.4577	0.4975	0.4768
Add both training/test time augmentation	0.4581	0.5293	**0.4911**

In our method, we select channel 4 to 7 in GHI as the original input according to the microphysical properties of convection. We also conduct an ablation experiment to illustrate the influence of channel selection. Results in Table 4 show that the inputs of these four channels are indispensable. Compared with using four channels as input, the model obtained by reducing any channel as input is significantly worse. The model with relatively better performance is the removal of the channel 5 (using channels 4, 6, 7 as input), and the F_1-measure obtained is 0.4676, 0.0235 lower than the original input. The worst performance is the removal of the channel 4, as a result, the F_1-measure is only 0.4002, 0.0909 lower than the original input. This may be due to the partial overlap between the observation of channel 5 and channel 4. The observation of channel 5 on low clouds is poor and the amount of information is insufficient, resulting in a greater impact of eliminating channel 4 than channel 5.

Table 4. Ablation study of channel selection.

Input	Precision	Recall	F_1-measure
Original input (channel 4 to 7)	0.4581	0.5293	**0.4911**
Remove channel 4	0.3606	0.4497	0.4002
Remove channel 5	0.3880	0.5883	0.4676
Remove channel 6	0.4370	0.4351	0.4361
Remove channel 7	0.4421	0.4793	0.4600

Figure 4 shows a typical example of the detection results of our Convection-UNet on June 17, 2022. The results of four UTC moments (00:30, 03:30, 06:30 and 09:30) are displayed from left to right. The background image in the result is visible imagery, while red pixels indicate true positives, blue pixels are false alarms, green pixels are misses, and yellow lines are national and provincial boundaries. It can be seen that our results can basically cover a large area of convection, the false alarms and misses mainly occur at the boundary of convection. In addition, our method can detect convective clouds when they are rising as overshooting tops, during this period, clouds usually show clear bubbling and lumpy-like textures on visible imagery. Therefore, the detection effect of overshooting tops confirms that the modeling of spatial context information of CNN is very important for the convection detection task.

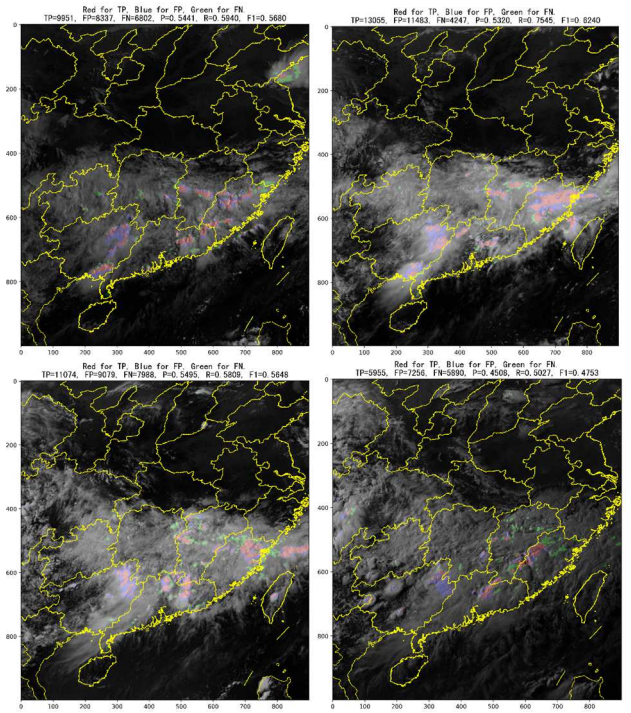

Figure 4. Visualization of results at specific moments. we select four moments on June 17, 2022 (00:30, 03:30, 06:30, and 09:30 UTC time from top left to bottom right respectively). Red pixels represent TP, blue pixels represent FP, green pixels represent FN, and yellow lines are provincial and national boundaries.

V. CONCLUSION

Motivated by the success of deep learning methods and their applications to computer vision, in this article, we propose a deep learning-based architecture Convection-UNet to detect convection. For the FY-4B GHI data, we discuss the scheme of channel selection in detail, then build a deep neural network Convection-UNet to automatically extract spatial context features and achieve end-to-end learning. Compared with the traditional channel selection combined with threshold filtering methods, the detection results are greatly improved. At the same time, we demonstrate that our channel selection and data augmentation strategy are effective. However, the development of convection is a dynamic process. Considering that GHI can provide data with a frequency of 1 minute, it is of great significance to introduce high time resolution information. In addition, the experiment uses visible imagery which has no effect on detecting convection at night. These problems are worth improving in further extended study areas.

ACKNOWLEDGMENT

This work was supported by the National Natural Science Foundation of China (NSFC) under Grant No. 62071469 and No. 71621002, Fengyun Application Pioneering Project(FY-APP) FY-APP-ZX-2022.0218.

REFERENCES

[1] Soriano L R, De Pablo F, Díez E G. Relationship between convective precipitation and cloud-to-ground lightning in the Iberian Peninsula[J]. Monthly weather review, 2001, 129(12):

2998-3003.

[2] Boccippio D J, Cummins K L, Christian H J, et al. Combined satellite-and surface-based estimation of the intracloud–cloud-to-ground lightning ratio over the continental United States[J]. Monthly Weather Review, 2001, 129(1): 108-122.

[3] Ivers L C, Ryan E T. Infectious diseases of severe weather-related and flood-related natural disasters[J]. Current opinion in infectious diseases, 2006, 19(5): 408-414.

[4] Mecikalski J R, Rosenfeld D, Manzato A. Evaluation of geostationary satellite observations and the development of a 1–2 h prediction model for future storm intensity[J]. Journal of Geophysical Research: Atmospheres, 2016, 121(11): 6374-6392.

[5] Chen D, Guo J, Yao D, et al. Elucidating the life cycle of warm-season mesoscale convective systems in eastern China from the Himawari-8 geostationary satellite[J]. Remote Sensing, 2020, 12(14): 2307.

[6] Maddox R A. Mesoscale convective complexes[J]. Bulletin of the American Meteorological Society, 1980: 1374-1387.

[7] Setvák M, Rabin R M, Wang P K. Contribution of the MODIS instrument to observations of deep convective storms and stratospheric moisture detection in GOES and MSG imagery[J]. Atmospheric Research, 2007, 83(2-4): 505-518.

[8] Mecikalski J R, Bedka K M. Forecasting convective initiation by monitoring the evolution of moving cumulus in daytime GOES imagery[J]. Monthly Weather Review, 2006, 134(1): 49-78.

[9] Sieglaff J M, Cronce L M, Feltz W F, et al. Nowcasting convective storm initiation using satellite-based box-averaged cloud-top cooling and cloud-type trends[J]. Journal of applied meteorology and climatology, 2011, 50(1): 110-126.

[10] Mathon V, Laurent H, Lebel T. Mesoscale convective system rainfall in the Sahel[J]. Journal of applied meteorology, 2002, 41(11): 1081-1092.

[11] LeCun Y, Bengio Y, Hinton G. Deep learning[J]. nature, 2015, 521(7553): 436-444.

[12] Lee Y, Kummerow C D, Ebert-Uphoff I. Applying machine learning methods to detect convection using Geostationary Operational Environmental Satellite-16 (GOES-16) advanced baseline imager (ABI) data[J]. Atmospheric Measurement Techniques, 2021, 14(4): 2699-2716.

[13] Kim M, Lee J, Im J. Deep learning-based monitoring of overshooting cloud tops from geostationary satellite data[J]. GIScience & Remote Sensing, 2018, 55(5): 763-792.

[14] Kim M, Im J, Park H, et al. Detection of tropical overshooting cloud tops using Himawari-8 imagery[J]. Remote sensing, 2017, 9(7): 685.

[15] Lee J, Kim M, Im J, et al. Pre-trained feature aggregated deep learning-based monitoring of overshooting tops using multi-spectral channels of GeoKompsat-2A advanced meteorological imagery[J]. GIScience & Remote Sensing, 2021, 58(7): 1052-1071.

[16] Ronneberger O, Fischer P, Brox T. U-net: convolutional networks for biomedical image segmentation[C]//International Conference on Medical image computing and computer-assisted intervention. Springer, 2015: 234-241.

[17] Yang J, Zhang Z, Wei C, et al. Introducing the new generation of Chinese geostationary weather satellites, Fengyun-4[J]. Bulletin of the American Meteorological Society, 2017, 98(8): 1637-1658.

[18] Zhang P, Xu Z, Guan M, et al. Progress of fengyun meteorological satellites since 2020[J]. Chinese Journal of Space Science, 2022, 42(4): 724-732.

[19] Gao B C, Goetz A F, Wiscombe W J. Cirrus cloud detection from airborne imaging spectrometer data using the 1.38 μm water vapor band[J]. Geophysical Research Letters, 1993, 20(4): 301-304.

[20] King M D, Tsay S C, Platnick S E, et al. Cloud retrieval algorithms for MODIS: Optical thickness, effective particle radius, and thermodynamic phase[J]. MODIS Algorithm Theoretical Basis Document, 1997, 1997.

[21] Sun F, Li B, Min M, et al. Deep learning-based radar composite reflectivity factor estimations from fengyun-4a geostationary satellite observations[J]. Remote Sensing, 2021, 13(11): 2229.

[22] Roberts R D, Rutledge S. Nowcasting storm initiation and growth using GOES-8 and WSR-88D data[J]. Weather and Forecasting, 2003, 18(4): 562-584.

[23] Isensee F, Jäger P F, Kohl S A, et al. Automated design of deep learning methods for biomedical image segmentation[J]. arXiv preprint arXiv:1904.08128, 2019.

[24] Milletari F, Navab N, Ahmadi S A. V-net: fully convolutional neural networks for volumetric medical image segmentation[C]//2016 Fourth International Conference on 3D Vision (3DV). IEEE, 2016: 565-571.

[25] Kingma D P, Ba J. Adam: a method for stochastic optimization[J]. arXiv preprint arXiv:1412.6980, 2014.

[26] Schmetz J, Tjemkes S, Gube M, et al. Monitoring deep convection and convective overshooting with METEOSAT[J]. Advances in Space Research, 1997, 19(3): 433-441.